

This is the accepted manuscript made available via CHORUS. The article has been published as:

## Reduction of Transfer Threshold Energy for Laser-Induced Jetting of Liquids using Faraday Waves

Emre Turkoz, SeungYeon Kang, Xiaohan Du, Luc Deike, and Craig B. Arnold

Phys. Rev. Applied **11**, 054022 — Published 8 May 2019

DOI: [10.1103/PhysRevApplied.11.054022](https://doi.org/10.1103/PhysRevApplied.11.054022)

# Reduction of transfer threshold energy for laser-induced jetting of liquids using Faraday waves

Emre Turkoz,<sup>1</sup> SeungYeon Kang,<sup>1</sup> Xiaohan Du,<sup>1</sup> Luc Deike,<sup>1,2</sup> and Craig B. Arnold<sup>1,\*</sup>

<sup>1</sup>*Department of Mechanical and Aerospace Engineering,  
Princeton University, Princeton, NJ, 08544, USA*

<sup>2</sup>*Princeton Environmental Institute, Princeton University, Princeton, NJ, 08544, USA*

Flow-focusing is used in microfluidics to generate droplets that are smaller than the characteristic length scale of the flow geometry. Conventionally, flow-focusing takes place inside micrometer-sized channels due to capillary effects. In this study, we demonstrate that the transient meniscus profile created with Faraday waves on liquid films can enable flow-focusing. Using a magnetic shaker, we generate Faraday waves on a liquid film leading to flow-focusing which increases the resolution of a nozzle-less, jet-based printing technique called blister-actuated laser-induced forward transfer (BA-LIFT). We perform experiments to demonstrate how transient meniscus formation enables jetting at lower laser pulse energies than the threshold, and use numerical modeling to examine this process at smaller length scales relevant to printing applications.

## I. INTRODUCTION

Flow-focusing has been a well-known phenomenon in microfluidics to create small droplets using micrometer-sized channels [1, 2]. Recently, this phenomenon has been shown to result in very fast and thin jets from capillary tubes using a pressure impulse such as the absorption of a laser pulse [3] or the mechanical impact resulting from a coil gun [4]. Flow-focusing has also been integrated into inkjet printing to print highly viscous fluids from capillary tubes [5] and into blister-actuated forward transfer (BA-LIFT) [6], which is the method used in this study to generate liquid jets, to reduce the ejected droplet size by half.

In these conventional applications of flow-focusing, the liquid forms a steady meniscus profile at the liquid-air interface due to surface tension. The desired profile is created by adjusting the geometry in order for the surface tension effects to be enhanced. In this study, we use a new approach and create a transient meniscus profile on a liquid thin film surface to generate focused jets. This is achieved by generating Faraday waves [7] into a liquid thin film using a magnetic shaker. We use the BA-LIFT technique to create jets by directing the laser pulse onto the surface points corresponding to the trough of the Faraday wave on the liquid film. We investigate the resulting focused jets using both experimental and numerical techniques to compare with the results from the regular jets induced from a flat liquid film.

BA-LIFT is a nozzle-less jet based deposition technique where the energy of a laser pulse is converted into mechanical energy through a rapidly expanding blister on a solid thick film [8]. With a liquid layer coating the polymer layer, this rapid blister expansion provides the impulsive pressure gradient [9] for jet formation and material transfer. By forcing Faraday waves into the liquid film, we exploit the geometrical effect of the meniscus

shaped interface, so that the focused laser pulse leads to the formation of a focused jet.

Faraday waves are induced by vibrating a liquid container perpendicular to the liquid-air interface above a certain acceleration threshold for a given set of parameters including liquid density  $\rho_l$ , liquid dynamic viscosity  $\mu_l$ , liquid-air surface tension  $\gamma$ , and thickness of the liquid film  $H_f$  [10–12]. For our experiments, we work close to the instability threshold, and obtain a regular wave pattern with a wavelength corresponding at half the forcing frequency, both being related by the dispersion relation for gravity-capillary waves with a depth  $H_f$ ,

$$\omega^2 = \tanh(kH_f) \left[ \frac{\gamma}{\rho_l} k^3 + gk \right], \quad (1)$$

where  $\omega$  is the angular frequency,  $k = 2\pi/\lambda$  is the wavenumber, and  $g$  is the gravitational constant.

In this Research Article, we first show experimentally that Faraday waves make jetting possible for sub-threshold laser energies. We perform the experiments for relatively large liquid film thicknesses compared to conventional LIFT printing applications due to experimental limitations in generating Faraday waves with an electromagnetic shaker. We show experimentally that Faraday waves reduce the laser transfer threshold energy. To demonstrate the applicability of this technique for small length scales, we perform direct numerical simulations. We validate our numerical model for small and large liquid film thicknesses. Our results show that Faraday waves can lead to the ejection of smaller droplets and therefore increase the resolution of the printing process.

## II. EXPERIMENTS

The simplified schematic of our experimental setup is presented in Fig. 1a. A 7  $\mu\text{m}$  thick polyimide film is coated on a glass slide via spin coating. The liquid film (deionized water with 0.1 wt.% Triton X-100 surfactant

---

\* cbarnold@princeton.edu

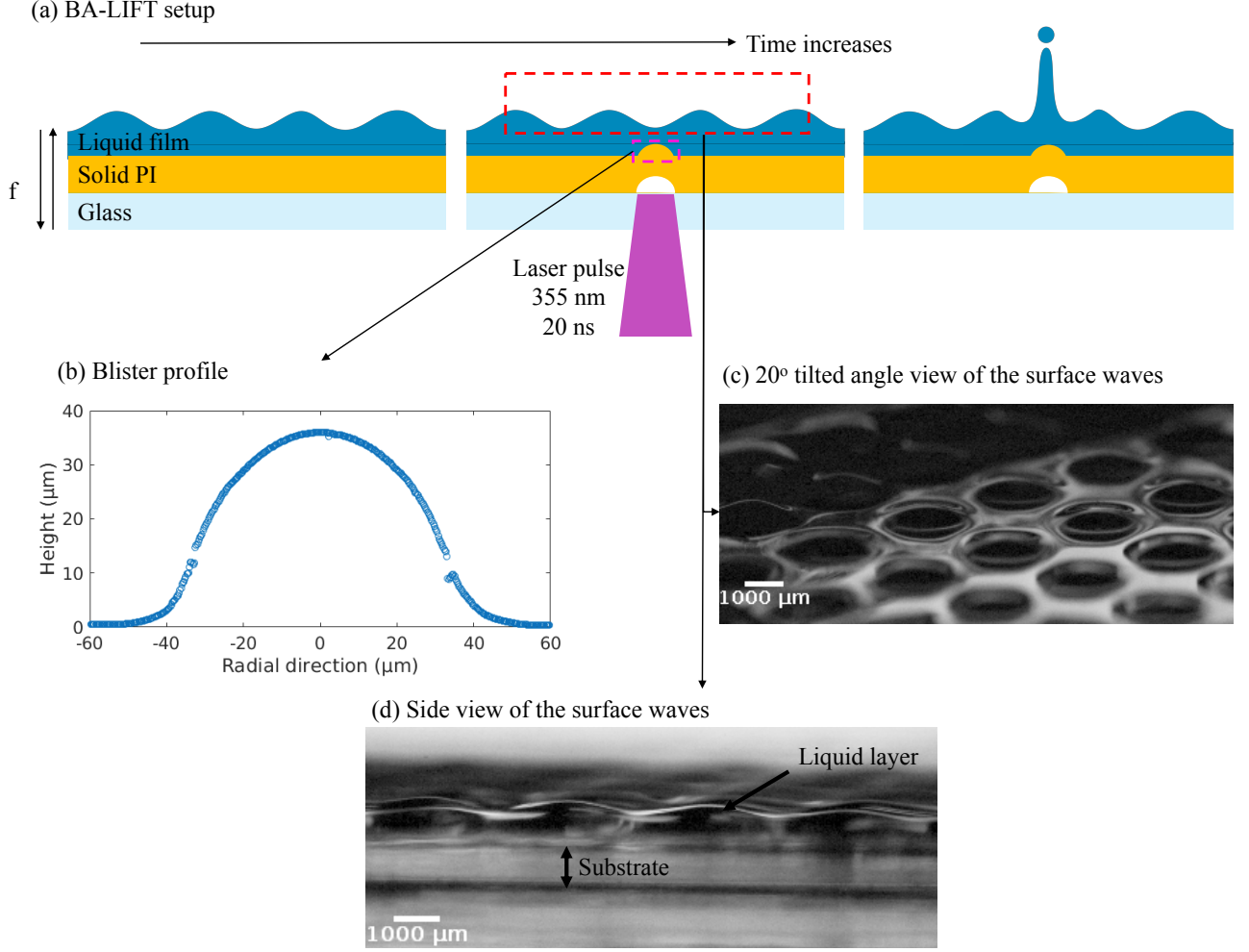


FIG. 1. Faraday wave transient meniscus is coupled with energy of the laser pulse to deposit materials. (a) Schematic of the experimental setup. The liquid film is coated on a solid polyimide 7- $\mu\text{m}$  thick film deposited on a transparent glass slide. We oscillate the substrate using a magnetic shaker. When the instability is generated with an acceleration above the critical value, we observe Faraday waves on the liquid surface. The laser pulse is then directed to the lowest point of the trough at the right time. (b) Dimensions of the blister measured using confocal microscopy. (c) The camera image of surface Faraday waves of a 160  $\mu\text{m}$  DI water layer on polyimide film from 20° tilted angle. The magnetic shaker frequency is set to 100 Hz. (d) Side images of the Faraday waves standing waves, which are used as transient meniscus for the BA-LIFT process.

(surface tension  $\gamma = 30.4 \text{ mN/m}$ , liquid dynamic viscosity  $\mu = 0.89 \text{ Pa.s}$ ) is coated by injecting the desired volume onto the sample and using magnetic shaker at low frequencies and amplitudes to spread the drop uniformly as a thick film. For the data presented in this study, the film thickness is  $H_f \approx 160 \mu\text{m}$ . The laser spot size is approximately 30  $\mu\text{m}$  and the pulse energy is measured as  $138 \pm 1.7 \mu\text{J}$ . The imaging of the resulting flow field is performed using a high-speed camera (Phantom v2012) with a macro lens (Nikon 200 mm f/4 AF-D) and an LED backlight. The substrate coated with the liquid film is oscillated vertically at 100 Hz using a magnetic shaker (Bruel & Kjaer LDS V455). The resulting Faraday waves are imaged with a slight angle as presented in Fig 1b.

The resulting Faraday waves have a wavelength of  $\approx 3.1 \text{ mm}$ , in agreement with the dispersion relation (1), and an amplitude of  $\approx 80 \mu\text{m}$ . Therefore, below the trough of the wave, the minimum ink thickness is 80  $\mu\text{m}$  while it is 240  $\mu\text{m}$  at the crest. For the flow-focusing to take place, it is crucial to synchronize the laser pulse to hit the trough of the wave when its amplitude is at maximum. This is done using a pulse generator so the laser pulse is sent at the right time corresponding to the end of the each period. To demonstrate that Faraday waves lower the transfer threshold energy, we present the images from a high-speed video of a transfer experiment. For the flat film case, the laser pulse does not deposit enough energy to the fluid and the resulting fluid motion does not yield jet formation as shown in Fig. 2. On

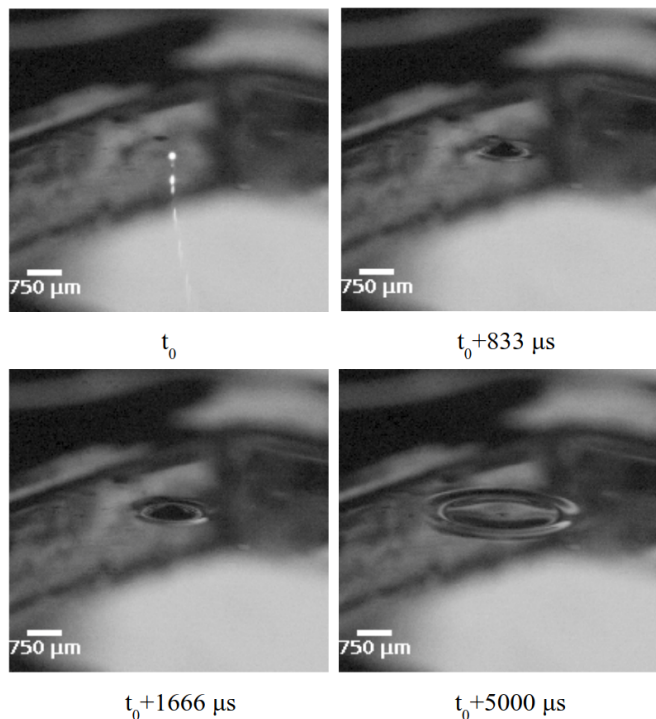


FIG. 2. Snapshots of the video for the flat film case. The plasma formed during the absorption of the laser pulse by the polyimide layer is apparent at the first snapshot denoted with  $t_0$ . The formed jet does not result in breakup.

the other hand, when we introduce Faraday waves, we see from Fig. 3 that the resulting jet breaks up into droplets. In this figure, at  $t = t_0$ , we see the reflection of the plasma created by the absorption of the laser pulse by the polyimide layer [13]. As time progresses by  $t = t_0 + 750 \mu s$ , we see the breakup of the first droplet from the jet. At  $t = t_0 + 1500 \mu s$ , we see the second droplet which retracts back to the liquid film. As a result, the resulting jet breaks up into two droplets while one of the droplets get ejected away from the thin film surface and the other one goes back to the thin film. The ejected droplet has the approximate radius of  $67 \mu m$ .

As shown in Fig. 3, Faraday waves make it possible for the jetting to take place at sub-threshold energies as observed previously with the steady meniscus configuration [6]. However, the question remains whether this improvement is due to a simple effective thickness reduction, or whether flow-focusing is playing a role as well. To answer this question and test this phenomenon at thinner liquid films, we perform numerical simulations of the BA-LIFT process. For instance, previous applications of BA-LIFT deals with the typical film thickness values on the order of  $\sim 5 \mu m$  [9, 14]. Such small thickness values are preferred for printing because the ejected droplet size from liquid films is proportional to the film thickness value [15].

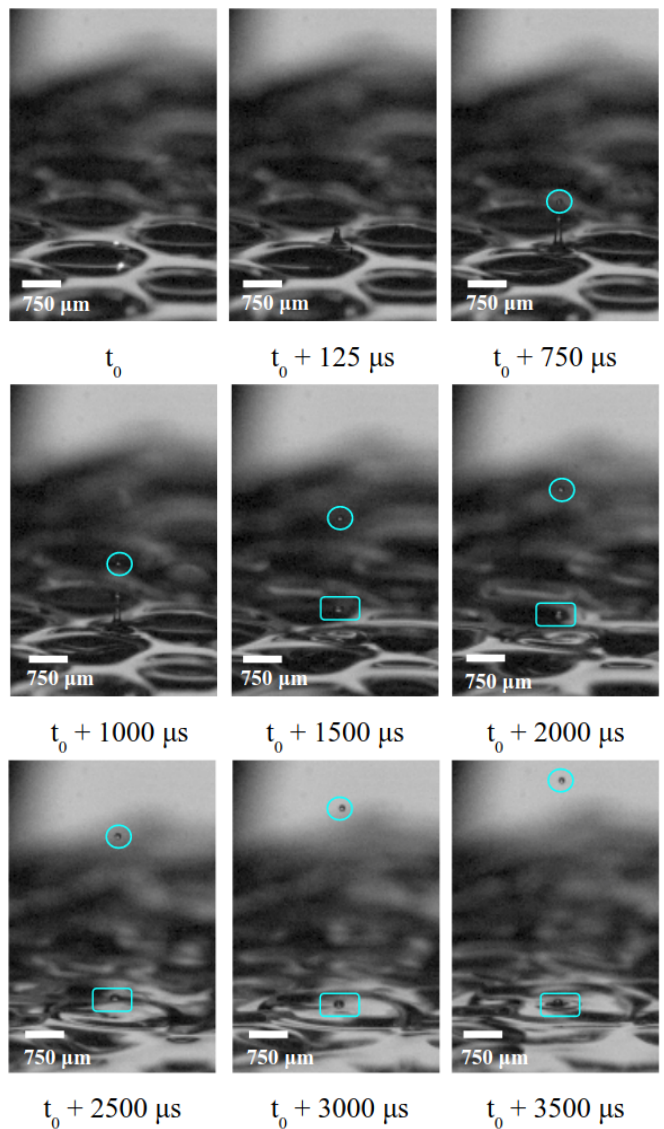


FIG. 3. Images from videos of the BA-LIFT process. The liquid layer thickness is  $160 \mu m$ . The laser pulse energy and spot size are the same as the flat film case. The videos are taken with 200,000 fps.  $t_0$  denotes the time when the laser pulse is sent to the sample. The jetting is possible with Faraday waves. The magnetic shaker frequency is 100 Hz. The resulting jet breaks up into multiple droplets. The blue circle on each figure points out the droplet ejected while the blue rectangle shows the droplet retracting back to the liquid film.

### III. NUMERICAL SIMULATIONS AND VALIDATION

We solve the axisymmetric two-phase incompressible Navier-Stokes equations with surface tension using the open source flow solver Basilisk [16, 17]. With this solver, the interface between the liquid layer and the ambient air is captured by a volume-of-fluid (VOF) method. These methods have been previously validated for various complex multiphase problems including splashing [18], break-

ing waves [19], bubble bursting [20], thinning of viscoelastic liquid bridges [21], and also the breakup of jets induced by BA-LIFT [22].

One of the most crucial parts of the model is the implementation of the boundary deformation during blister formation. The time-dependent blister profile  $\delta$  is given by [14] as  $\delta(r, E, t) = X(r, E)T(t)$ , where  $X(r, E)$  and  $T(t)$  define the energy-dependent ( $E$  in  $\mu\text{J}$ ) blister profile and the time dependence function, respectively. The blister profile is expressed as  $X(r, E) = H_0(E) \left(1 - (r/R_b(E))^2\right)^C$  (in  $\mu\text{m}$ ) and the time dependence function is expressed as  $T(t) = (2/\pi)\arctan(t/\tau_b)$ , where  $H_0(E) = -0.0093E^2 + 2.5708E - 9.2618$  is the laser energy-dependent blister height (in  $\mu\text{m}$ ),  $R_0(E) = 18.117\ln(E) - 12.887$  is the blister radius (in  $\mu\text{m}$ ),  $C$  is a shape coefficient, and  $\tau_b = 23.5 \cdot 10^{-9}$  s is the characteristic time scale for blister formation [23] for the 20 ns pulse laser used in this study.

The jetting and breakup of a liquid jet depend on the ambient air properties as well [24]. In addition to the blister deformation, the problem is governed by the dimensionless parameters  $\mu_a/\mu_l$ ,  $\rho_a/\rho_l$ ,  $\tau_b/t_c$ , and the Ohnesorge number  $\text{Oh} = \mu_l/\sqrt{\rho_l\gamma\bar{H}_f}$ , where  $t_c = \sqrt{\rho_l H_f^3/\gamma}$ .

We first present the snapshots from the simulation results for a flat film of 5  $\mu\text{m}$  with the laser pulse energy of 5.14  $\mu\text{J}$  in Fig. 4a-d obtained from simulations performed with the refinement approximately corresponding to 10.68 cells/ $\mu\text{m}$  resolution. We evaluate the blister height and radius with the formulas given above as  $H_0 = 3.7 \mu\text{m}$  and  $R_0 = 16.8 \mu\text{m}$ , respectively. The transferred droplet volume at this threshold energy is evaluated with increasing grid resolution. This result is presented in Fig. 4e. The grid convergence study is performed with an adaptive grid on a single node and multiple processors with MPI parallelization. Figure 4e shows that all of the cases converge numerically for the mesh size above 10 cells/ $\mu\text{m}$ .

We then validate our numerical simulations in the flat film case, by comparing the numerical results with the experimental results and previous computational work [14]. Figure 5 shows the ejected droplet volume from our Basilisk simulations, which reproduce the experimental data and earlier modeling results with great accuracy.

The validation presented in Fig. 4 and 5 is for a liquid film of 5  $\mu\text{m}$  thickness. Now, we test the validity of the numerical model with thicker films such as those used in the experiments described in Section II. To test the validity of the model for large ink thicknesses, we compare the numerical results with the experimental images of the BA-LIFT process with a 65- $\mu\text{m}$ -thick liquid film of a water-glycerol solution (80 wt.% water - 20 wt.% glycerol) with 0.1 wt.% Triton X-100 surfactant ( $\mu = 1.7$  mPa.s,  $\gamma = 30.4$  mN/m). We use the same laser pulse energy that creates the blister profile presented in Fig. 1b, where  $H_0(E) = 38 \mu\text{m}$ ,  $R_0(E) = 50 \mu\text{m}$ , and the shape factor  $C = 2.73$ . We note that the grid convergence study is performed for this configuration as well, and the same

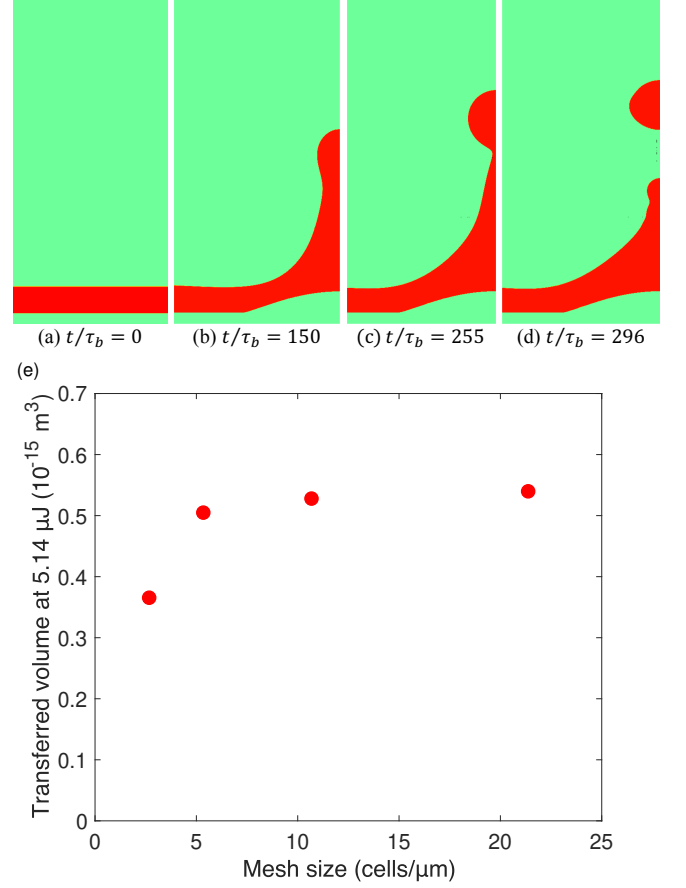


FIG. 4. Grid convergence of the numerical model implemented in the Basilisk open source flow solver for the flat film case. (a-d) The snapshots obtained from simulations performed with the refinement corresponding to 10.68 cells/ $\mu\text{m}$  resolution. (e) The grid convergence study is performed for an adaptive grid with MPI parallelization on multiple nodes and processors. Transferred droplet volume converges above 10 cells/ $\mu\text{m}$ .

resolution as the previous case ( $\sim 10$  cells/ $\mu\text{m}$ ) is employed. The grid refinement used in the previous section yields numerically converged results for this configuration as well.

Results of the jet formation from both the experiment and simulation are presented in Fig. 6. For these high-speed videos, we used the same high-speed camera with a microscope (InfiniTube with a Mitutoyo 10 $\times$  objective) for higher resolution. It is seen from the high-speed video images that while initially the numerical jet is shorter, the features of the jet are very similar for both jets. While the experimental images show an elongated neck right before droplet breakup as seen in Fig. 6b and 6c, the neck is shorter for the simulated case. The ejected droplet has the diameter of 38.8  $\mu\text{m}$  as measured from the images. The simulations yield the droplet diameter to be 36.8  $\mu\text{m}$ , which is very close to the experimentally obtained value.

High-speed videos allow us to record the length of the



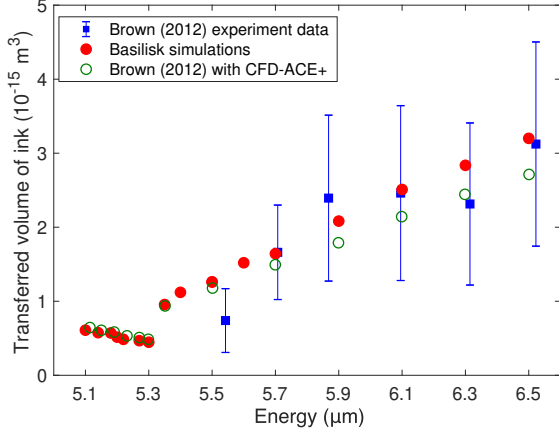


FIG. 5. Validation of the numerical results with the experiments. We observe that Basilisk simulations produce results that are within the standard deviation of the experimental results and in good agreement with the modeling presented in [14].

jet measured from the surface at each time step. The evolution of jet length as a function of time from the experiment and the numerical simulation is presented in Fig. 6e. While the simulation results do not follow the experimental curve exactly, they succeed in representing the main features of the jet. According to the simulations, the breakup takes place at  $t = 44.6 \mu\text{s}$ , which is very close to the experimentally obtained value of  $t \approx 48.5 \mu\text{s}$ . We note that while the simulations predict the droplet size and time of breakup in very good agreement with the laboratory experiments, the jet dynamics presented in Fig. 6e exhibit some difference. These differences are likely due to the formulation of the solid boundary deformation. The time dependence of the blister profile presented in our previous work [14] and used here assumes that the blister expands monotonically while we showed in our previous studies [13] that the blister height and volume exhibit oscillations after the blister reaches its full length. Furthermore, the shape of the blister also changes dynamically during the expansion (during first  $\sim 25 \text{ ns}$ ), where the blister initially has a pointed tip which then relaxes to a Gaussian profile. Experiments and numerical simulations of jetting in other context have demonstrated an extreme sensitivity in the geometry of the focusing process leading to the jet formation [20, 25], so that the uncertainties in the blister dynamics directly affect the resulting liquid jet dynamics.

This completes the validation of the numerical model developed for this study. We note that there are no fitting parameters for the direct numerical simulations, and the results from the numerical model show good agreement with the experiments.

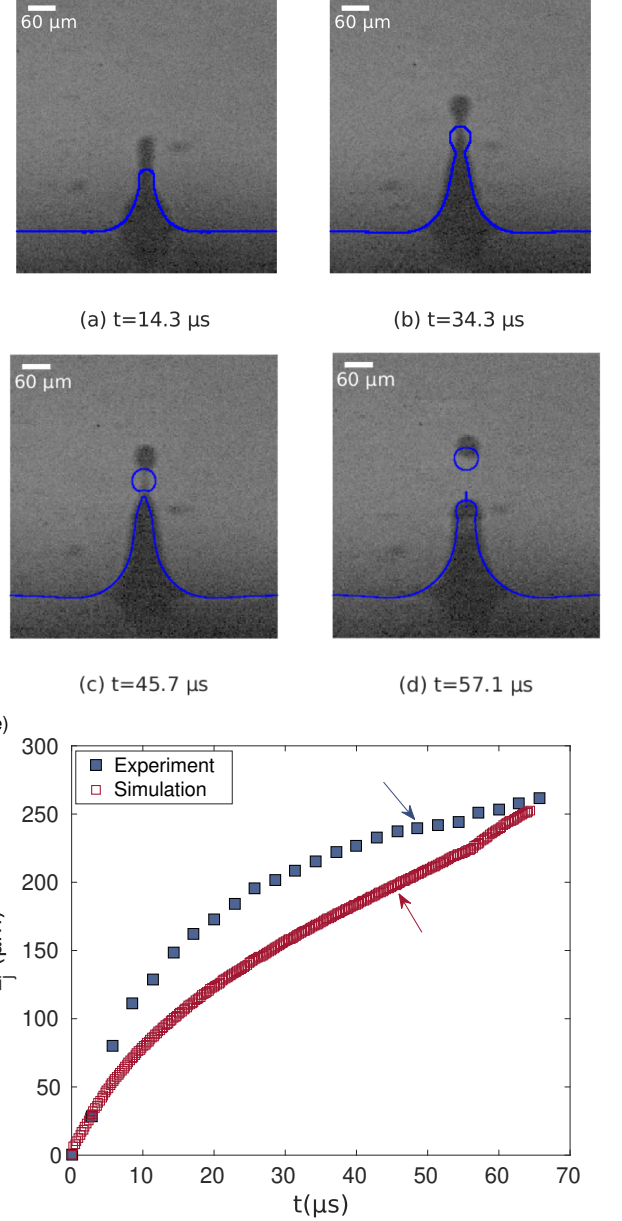


FIG. 6. Validation of the numerical model with high-speed video images of experiments. (a-d) Superposition of experimental and numerical profiles. The ejected droplet diameter from the simulations is  $36.8 \mu\text{m}$ , which is very close to the experimental value of  $38.8 \mu\text{m}$ . (e) Jet length  $L_j$  as a function of time  $t$  obtained from experiments and simulations for the same configuration as presented in (a-d). The colored arrows indicate the moment of breakup for the each case.

#### IV. RESULTS

Now, we simulate the effect of Faraday waves at small length scales relevant to printing applications. We consider Faraday waves with the wavelength of  $\lambda_c = 150 \mu\text{m}$ . To represent the Faraday waves in our model,

we represent the surface profile as an axially symmetric sinusoidal function which can be formulated as  $H_f + a \cos[(2\pi/\lambda_c)(\lambda_c/2 - r)]$ , where  $a$  is the wave amplitude,  $r$  is the radial coordinate, and  $H_f = 5 \mu\text{m}$  is the average film thickness value we picked in accordance with previous applications [9, 14]. This sinusoidal shape assumed for the Faraday waves matches the solutions of the governing equations and wave patterns that are experimentally observed in the literature [10, 26, 27]. Note that the wave simulated in this section has very similar depth to wavelength ratio with the one considered for the thick film in Section II, where  $H_f/\lambda = 0.05$  for the thick film, and  $H_f/\lambda_c = 0.033$  for the thin film in this section. So in both cases, we are in an intermediate depth configuration. We only consider the geometrical effect of Faraday waves because the wave dynamics takes place at a time scale much slower than the laser-induced blister formation,  $1/\omega \gg \tau_b$ . The minimum thickness value along the wave profile corresponds to  $r = 0$  with  $H_{min} = H_f - a$ . We sweep different Faraday wave amplitudes from  $0.5 \mu\text{m}$  to  $2.5 \mu\text{m}$ . We picked  $a = 2.5 \mu\text{m}$  as the largest amplitude as this value satisfies the criterion  $a/\lambda_c < 0.1$ , which we experimentally observed to lead to spatially stable Faraday waves.

An example of the jet dynamics and the jet profiles is presented in Fig. 7. In this figure, the flat film case  $a = 0.0 \mu\text{m}$  at the transfer threshold energy  $E_{th} = 5.09 \mu\text{J}$ , shown in blue, is presented with the Faraday wave case  $a = 2.5 \mu\text{m}$  at a lower laser pulse energy of  $E = 4.95 \mu\text{J}$ , shown in red. For each of these cases, the black curve at the bottom denotes the interface between the liquid film and the solid polyimide layer, and the colored curve at the top denotes the interface between the liquid film and air. Figure 7a shows the initial case where the liquid-solid interface is flat and the blister formation is yet to take place. After blisters form (Fig. 7a-b), the liquid films yield jet formation that results in breakup (Fig. 7c-f). We see from this figure that the droplet ejected using Faraday waves is smaller and faster compared to the one ejected from the flat film (Fig. 7e-f).

Figure 8 shows results for the Faraday wave configurations for increasing laser pulse energy and increasing wave amplitude. While the filled symbols denote single drop ejections per laser pulse, the open symbols represent the multiple drop cases. Ejecting a single drop per pulse is the preferred method for printing, and the lowest deposited droplet volume is obtained at the transition from single drop to multiple drop regimes [14]. This corresponds to  $5.22 \mu\text{J}$  for the no Faraday wave ( $a = 0 \mu\text{m}$ ) case with the ejected droplet size of  $4.72 \mu\text{m}$ . However, when a Faraday wave of the amplitude  $a = 2.5 \mu\text{m}$  is introduced into the system, the resulting configuration with the minimum film thickness  $H_{min} = 2.5 \mu\text{m}$  results in a smaller droplet with a radius of  $4.04 \mu\text{m}$  with  $5.02 \mu\text{J}$  laser pulse. This means that Faraday waves and the resulting flow-focusing effect can achieve approximately 40% reduction of volume, which is close to the 50% improvement we previously demonstrated with

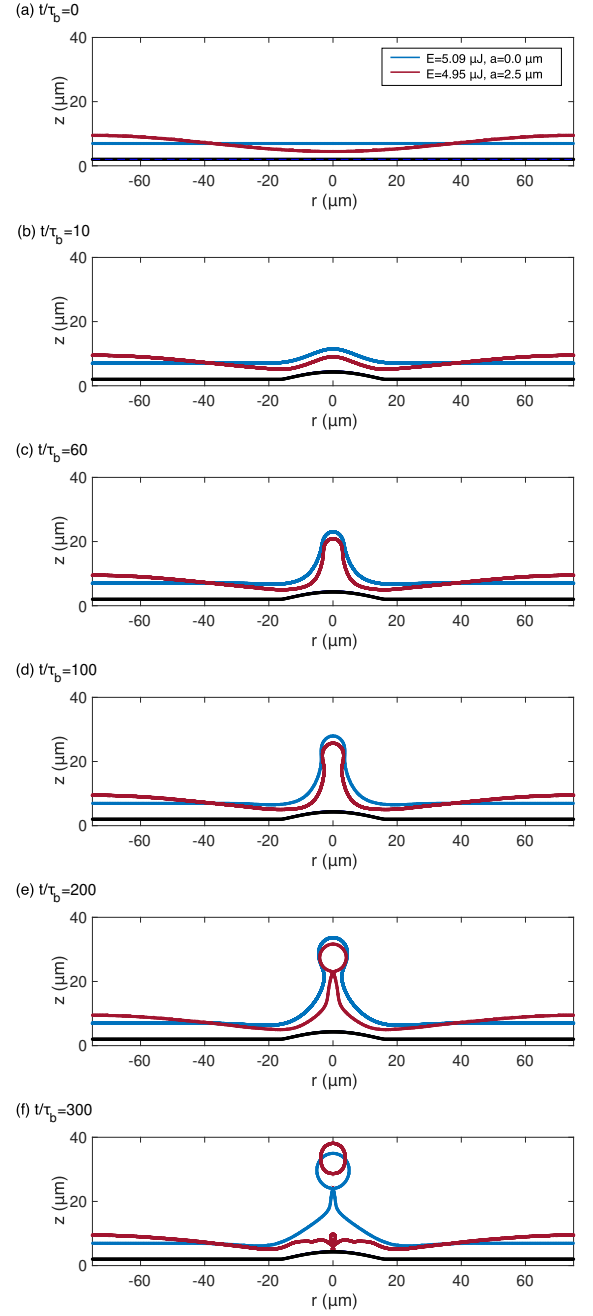


FIG. 7. Snapshots of the jet profiles from numerical simulations. Blue curves represent the flat film case ( $E = 5.09 \mu\text{J}$ ) while red curves represent the case with  $a = 2.5 \mu\text{m}$  Faraday wave amplitude ( $E = 4.95 \mu\text{J}$ ). The two overlapped profiles at the bottom denote the interface between the liquid and the blister while the two profiles at the top represent the interface between the liquid and air.

steady meniscus formation [6]. The inset figure presents the reduction in transfer threshold energy as a function of Faraday wave amplitude in Fig. 8. We see that the threshold energy converges to a value lower than the flat film threshold energy as the Faraday wave amplitude is increased.

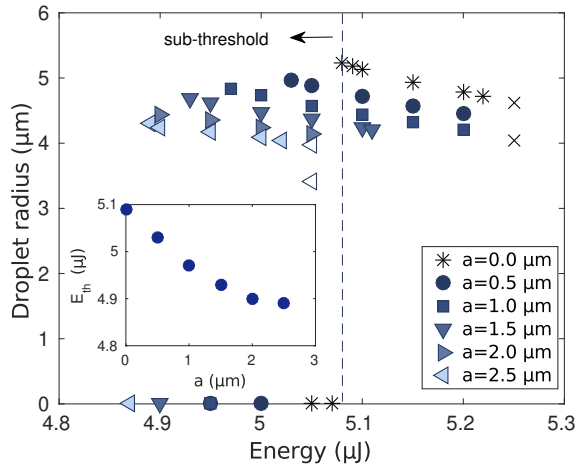


FIG. 8. Results of the Basilisk simulations. Flow-focusing effect due to Faraday waves lowers the transfer threshold laser energy. Filled symbols denote single drop ejections and empty symbols denote multiple-drop ejections. For flat film cases ( $a = 0.0 \mu\text{m}$ ), the single drop ejections are represented with (\*) while the multiple-drop case is represented with ( $\times$ ). Single drop ejections obtained using Faraday waves smaller droplets compared to the no Faraday wave case. The inset figure shows the reduction in transfer threshold energy as a function of the Faraday wave amplitude.

The average film thickness value of  $H_f = 5 \mu\text{m}$  has the transfer threshold energy of  $5.09 \mu\text{J}$  with no additional Faraday wave as shown in Fig. 8. This threshold energy produces a droplet with a radius of  $5.23 \mu\text{m}$ . We also indicate the threshold laser energy with a vertical dashed line for the no Faraday wave case. The introduction of Faraday waves makes it possible for the ejection to take place at lower energies than this threshold energy. Thus, Fig. 8 shows that the creation of a shallow meniscus using Faraday waves improves the process by lowering the threshold energy and ejected droplet size.

## V. DISCUSSIONS AND CONCLUSION

We show here that Faraday waves can create meniscus shaped interfaces and lead to flow-focusing when coupled with an impulsive pressure such as provided by the BA-LIFT process. This technique has a major advantage over conventional flow-focusing applications as the formation of the meniscus does not depend on the wettability of the liquid to solid walls. Faraday waves can be generated on liquid thick films without confinement.

It is important to note that the viscous dissipation

term can be important for Faraday waves generated using liquids with high viscosity values. The viscous dissipation rate  $\delta$  for a wave of frequency  $\omega$  is proportional to  $\delta \sim \nu k^2 \omega^{-1}$ , where  $\nu = \mu/\rho$  is the kinematic viscosity [28, 29]. It is still possible to generate Faraday waves with highly viscous liquids; however, a larger acceleration is required to overcome the viscous dissipation as the instability threshold depends on viscosity and frequency [30]. Exciting Faraday waves of  $150 \mu\text{m}$  wavelength would require forcing at  $\sim 10,000 \text{ Hz}$ .

An important aspect of inducing jets with flow-focusing is the determination of the relationship between the ejected droplet size and the relevant parameters. To our knowledge, there is no established theory that relates the droplet size to the meniscus size. The previous literature on flow-focusing [3, 31] has focused on the scaling of jet velocity with capillary diameter, pressure gradient and surface tension. We have experimentally observed that the ejected droplet size decreases as the pressure impulse is increased, however, the resulting jets result in multiple droplets. In addition, numerical simulations, as presented in Fig. 8, indicate that as the amplitude to the wavelength ratio ( $a/\lambda_c$ ) is increased, the ejected droplets are smaller. However, a more systematic study can be performed in the future to see the affect of the wavelength on the ejected droplet size.

In this Research Article, we show experimentally and numerically that Faraday waves enhance the jetting process during BA-LIFT by lowering the transfer threshold energy and decreasing the ejected droplet radius. Transient meniscus formation leads to flow-focusing as steady meniscus formation does [5, 6]. In this study, we couple the geometrical effects due to meniscus-shaped interface with the laser energy to print smaller droplets using flow-focusing. We believe that this study will pave the way to the development of new laser jetting techniques that incorporate multiple forms of energy to enhance droplet resolution.

## ACKNOWLEDGMENTS

We acknowledge the funding by National Science Foundation (NSF) through a Materials Research Science and Engineering Center program (DMR-1420541). The computations were partially performed using allocation TGOCE140023 to L.D. from the Extreme Science and Engineering Discovery Environment (XSEDE), supported by NSF grant no. ACI-1053575, and using Princeton Research Computing resources, including the Princeton Institute for Computational Science and Engineering and the High Performance Computing Center. We also acknowledge the funding by the Princeton University Schmidt Fund.



- [2] H. A. Stone, A. D. Stroock, and A. Ajdari, “Engineering flows in small devices: microfluidics toward a lab-on-a-chip,” *Annual Review of Fluid Mechanics* **36**, 381–411 (2004).
- [3] Y. Tagawa, N. Oudalov, C. W. Visser, I. R. Peters, D. van der Meer, C. Sun, A. Prosperetti, and D. Lohse, “Highly focused supersonic microjets,” *Physical Review X* **2**, 031002 (2012).
- [4] H. Onuki, Y. Oi, and Y. Tagawa, “Microjet generator for highly viscous fluids,” *Physical Review Applied* **9**, 014035 (2018).
- [5] P. Delrot, M. A. Modestino, F. Gallaire, D. Psaltis, and C. Moser, “Inkjet printing of viscous monodisperse microdroplets by laser-induced flow focusing,” *Physical Review Applied* **6**, 024003 (2016).
- [6] E. Turkoz, S. Kang, L. Deike, and C. B. Arnold, “Sub-threshold laser jetting via flow-focusing in laser-induced forward transfer,” *Physical Review Fluids* **3**, 082201 (2018).
- [7] M. Faraday, “Xvii. on a peculiar class of acoustical figures; and on certain forms assumed by groups of particles upon vibrating elastic surfaces,” *Philosophical transactions of the Royal Society of London* **121**, 299–340 (1831).
- [8] E. Turkoz, R. Fardel, and C. B. Arnold, “Advances in blister-actuated laser-induced forward transfer (ba-lift),” *Laser Printing of Functional Materials: 3D Microfabrication, Electronics and Biomedicine* (2018).
- [9] C. F. Brasz, C. B. Arnold, H. A. Stone, and J. R. Lister, “Early-time free-surface flow driven by a deforming boundary,” *Journal of Fluid Mechanics* **767**, 811–841 (2015).
- [10] S. Douady, “Experimental study of the faraday instability,” *Journal of Fluid Mechanics* **221**, 383–409 (1990).
- [11] K. Kumar, “Linear theory of faraday instability in viscous liquids,” *Proceedings of the Royal Society of London A* **452**, 1113–1126 (1996).
- [12] B. J. Gluckman, C. B. Arnold, and J. P. Gollub, “Statistical studies of chaotic wave patterns,” *Physical Review E* **51**, 1128 (1995).
- [13] M. S. Brown, N. T. Kattamis, and C. B. Arnold, “Time-resolved study of polyimide absorption layers for blister-actuated laser-induced forward transfer,” *Journal of Applied Physics* **107**, 083103 (2010).
- [14] M. S. Brown, C. F. Brasz, Y. Ventikos, and C. B. Arnold, “Impulsively actuated jets from thin liquid films for high-resolution printing applications,” *Journal of Fluid Mechanics* **709**, 341–370 (2012).
- [15] E. Turkoz, A. Perazzo, H. Kim, H. A. Stone, and C. B. Arnold, “Impulsively induced jets from viscoelastic films for high-resolution printing,” *Physical Review Letters* **120**, 074501 (2018).
- [16] S. Popinet, “A quadtree-adaptive multigrid solver for the serre-green-naghdi equations,” *Journal of Computational Physics* **302**, 336–358 (2015).
- [17] S. Popinet, “Numerical models of surface tension,” *Annual Review of Fluid Mechanics* (2018).
- [18] C. J. Howland, A. Antkowiak, J. R. Castrejón-Pita, S. D. Howison, J. M. Oliver, R. W. Style, and A. A. Castrejón-Pita, “Its harder to splash on soft solids,” *Physical Review Letters* **117**, 184502 (2016).
- [19] L. Deike, W. K. Melville, and S. Popinet, “Air entrainment and bubble statistics in breaking waves,” *Journal of Fluid Mechanics* **801**, 91–129 (2016).
- [20] L. Deike, E. Ghabache, G. Liger-Belair, A. K. Das, S. Zaleski, S. Popinet, and T. Séon, “Dynamics of jets produced by bursting bubbles,” *Physical Review Fluids* **3**, 013603 (2018).
- [21] E. Turkoz, J. M. Lopez-Herrera, J. Eggers, C. B. Arnold, and L. Deike, “Axisymmetric simulation of viscoelastic filament thinning with the oldroyd-b model,” *Journal of Fluid Mechanics* **851** (2018).
- [22] C. F. Brasz, J. H. Yang, and C. B. Arnold, “Tilting of adjacent laser-induced liquid jets,” *Microfluidics and Nanofluidics* **18**, 185–197 (2015).
- [23] N. T. Kattamis, M. S. Brown, and C. B. Arnold, “Finite element analysis of blister formation in laser-induced forward transfer,” *Journal of Materials Research* **26**, 2438–2449 (2011).
- [24] H. A. Stone, “Dynamics of drop deformation and breakup in viscous fluids,” *Annual Review of Fluid Mechanics* **26**, 65–102 (1994).
- [25] C.-Y. Lai, J. Eggers, and L. Deike, “Bubble bursting: universal cavity and jet profiles,” *Physical Review Letters* **121**, 144501 (2018).
- [26] S. Douady and S. Fauve, “Pattern selection in faraday instability,” *EPL (Europhysics Letters)* **6**, 221 (1988).
- [27] W. S. Edwards and S. Fauve, “Patterns and quasipatterns in the faraday experiment,” *Journal of Fluid Mechanics* **278**, 123–148 (1994).
- [28] J. W. Miles, “Surface-wave damping in closed basins,” *Proceedings of the Royal Society of London. Series A. Mathematical and Physical Sciences* **297**, 459–475 (1967).
- [29] L. Deike, M. Berhanu, and E. Falcon, “Decay of capillary wave turbulence,” *Physical Review E* **85**, 066311 (2012).
- [30] S. Kumar, “Mechanism for the faraday instability in viscous liquids,” *Physical Review E* **62**, 1416 (2000).
- [31] I. R. Peters, Y. Tagawa, N. Oudalov, C. Sun, A. Prosperetti, D. Lohse, and D. van der Meer, “Highly focused supersonic microjets: numerical simulations,” *Journal of Fluid Mechanics* **719**, 587–605 (2013).